ESTIMATING PARAMETERS OF DYNAMIC FUEL INJECTION SYSTEM MODELS

W. EGARTNER* AND H. OFNER†

Abstract.
A parameter estimation strategy based on dynamic measurements in fuel injection line-nozzle systems is presented. The goal is to capture essential dynamic flow properties. Commonly used 1-D hydraulic models are investigated with respect to identifiability of parameters like geometry properties, flow loss, cavitation phenomena, velocity of sound and kinetic viscosity. Measurements with both diesel and dimethyl ether are considered. Some models give both identifiable and physically reasonable parameters. Others reveal the infeasibility of simplifying assumptions. Possible improvements are discussed.

Key words. 1-D hydraulic models of line-nozzle systems for direct fuel injection; laminar, turbulent and cavitating flow in orifices; dynamic increase of friction in pipes with circular cross section. Integro-partial differential equations of Volterra type. Nonlinear parameter estimation.

AMS subject classifications.
45K05, 76D99.

1. Introduction. The demand for efficiency improvement of fuel injection systems rises the need for a deeper understanding of their dynamic flow properties. As measurements do not give direct access to these properties, parameter estimation comes into play.

In this paper, we focus on the investigation of 1-D hydraulic models similar to those presented in [4, 8, 15]. In order to derive reliable results, we want to find parameterizations that yield sharp estimates and a clear match between parameters and physical properties. Special attention is drawn on the impact of noisy data and measurement calibration errors.

As there is significant covariance of the orifice and pipe viscosity parameters, we estimate them separately.

So after a brief introduction to parameter estimation in §2, we dedicate §3 to parameter estimation of orifice models for laminar, turbulent and cavitating flow. In this case we arrive at parameters that allow quite straightforward physical interpretation based on both practical experience and theoretical considerations.

In §4 we identify kinetic flow viscosity and velocity of sound from pressure measurements along the injection line. This leads to a thorough discussion about the impacts of certain model simplifications. We also report how the pipe model's integro-partial differential equations are solved by a new efficient technique. This is essential in view of the numerous runs needed for the reliability check of the computed results.

In §5 we outline ideas one can follow in order to use the results of the previous sections to analyse a full line-nozzle system.

2. Parameter estimation strategy. In this section we want to outline the central ideas we follow in parameter estimation and model generation.

To maintain simplicity, we assume that measurement errors including propagated ones are independent and normally distributed. Based on this assumption, we com-

*IWR, University of Heidelberg, Germany
†AVL List GmbH, Graz, Austria

pute parameter estimates θ^* by minimizing the Least Squares functional

$$\chi^2(\theta) := \frac{1}{\sigma_y^2 + \sigma_f^2} \sum_{i=1}^{n} (y_i - f(x_i, \theta))^2 , \tag{2.1}$$

where σ_y^2, σ_f^2 are the *averaged* variances of the measurement errors of our data y and x, the latter being propagated through the model f.

The minimization is carried out by the Levenberg-Marquardt implementation method [9] by Moré [11] (`LMDIF` of MINPACK [12]).

As this is a local method (i. e. it finds local minima, not global ones), we perform optimization runs with various starting points following practical considerations. If one of the solutions has a significantly lower χ^2-value than the others, it is supposed the global solution. If we have substantially different solution points with similar χ^2-values, however, we have to question identifiability.

Once having found an estimate we specify the nature of fluctuations of the *residuals* $y_i - f(x_i, \theta)$, i. e. we check their distribution. Single outliers are removed and minimization is repeated. If the model responses reveal a clear trend off the data y, however, we consider possible model improvements.

The next step is to clarify the relationship between the parameters and the measurements. We want to know how *accurate* the parameters can be determined from the given measurement information. For that purpose, we have to reconstruct *confidence regions*, i. e. the chi-square boundaries

$$\chi^2(\theta) \le \chi^2(\theta^*)(1 + \frac{1}{\nu}) \tag{2.2}$$

with $\nu = n - m$. As a rule of thumb, the boundary (2.2) contains the parameters to a confidence level of about 0.7 under the assumption that the model fits well [16], which is needed in view of the unknown variances. This means that at this point we only know about the shape of the confidence regions, which gives us a means to find a better parameterization. Their actual size depends on the validity of the model's good-fit assumption and is therefore unknown. We will go into this in the last paragraph of this section.

For confidence region reconstruction Monte-Carlo type methods or constant-chi-square boundaries are used. Both methods are very expensive, but due to the significantly nonlinear nature of both the model and the measured data we do not see whether linear theory (i. e. analyzing covariance matrices $J^\top J$ with J being the model's local Jacobian) gives reliable information or not.

Now we are in a position to also get some insight in the influence of measurement errors. For that purpose, introduce error control parameters ξ so that we get expanded confidence regions

$$\chi^2(\theta, \xi) \le \chi^2(\theta^*, \xi^*)(1 + \frac{1}{\nu}) . \tag{2.3}$$

We feel that the *projection* of this region onto the parameter space gives more information about the reliability of the parameters than its mere *intersection* 2.2 with a fixed error value hyperspace.

An example is shown in figure 3.1, where the projection is denoted σ_ζ and the region due to (2.2) would be the intersection of the expanded region with some arbitrary $\alpha = const.$-line.

Having performed the above steps, we may have arrived at a mathematically reliable parameter set. Now we have to check whether these parameters are *physically reasonable*. As we put strong emphasis on interpretability when choosing our parameterization, the physical validation will be straightforward in most cases. Sometimes it can be performed by both theoretical considerations or a judgement based on measured data of more simple, though comparable situations (e. g. for steady flow).

So now that we (maybe) have found the best parameterization and the best parameters what about the a-priori good-fit assumption of the model as such? We believe the best way to cope with that is to start with a rather simplistic model, then to refine it step by step with additional features and to observe and protocol what is going on. With this strategy we get get some idea about essential model properties and their effect on the parameter estimates.

3. Orifice flow.

3.1. Models. Throughout this paper the term "orifice" denotes a location where kinetic energy dissipates. We are considering measurements at orifices with circular cross section, ring-shaped orifices and RSN nozzles with 5 sprayholes.

We neglect the influence of outer forces and inertia effects, where the latter assumption is motivated by investigations presented in [3]. As it is a common practice in computations of orifices in fuel injection systems, an average value for the density is introduced and the specific kinetic energies due to velocities are considered small compared to those due to pressure.

Under these assumptions the relationship between inlet and outlet pressures (p_{in}, p_{out} and the flow velocity u_0 in the orifice can be described as follows:

$$|p_{in}(t) - p_{out}(t)| \;=\; \frac{1}{2} \cdot \zeta(t) \cdot \rho \cdot u_0(t)^2 \;. \tag{3.1}$$

The friction factor $\zeta(t)$ is the function to be estimated. It can be related to any velocity u_0 within the orifice while most commonly it is associated to the velocity at the narrowest cross section.

We have measurements of $p_{in}(t)$ and $p_{out}(t)$ at discrete times, but we have no measurements of u_0. Instead, only the total volume per cycle is measured, which is u_0 integrated over time. Therefore, a large set of measurements at various operating points (such as pump load, pump speed and orifice diameter) is required in order to identify $\zeta(t)$.

In order to exploit existing knowlegde about loss coefficients (mostly motivated by steady-state measurements), we are going to represent $\zeta(t)$ as a parameterized function of the Reynolds number. The validity of the resulting parameterization is measured by the confidence intervals of the identified parameters.

From steady-state measurements the friction factor for *laminar* and *transitional* flow is observed to be a function of the Reynolds number Re. In practice, the pattern

$$\zeta(t) = \zeta_0 + \frac{\ell}{D_0}\left(\frac{a}{Re(t)^{\,b}} + c\right) \tag{3.2}$$

is commonly applied [5], where $Re(t) = u_0(t) \cdot D_0/\nu$. As the Reynolds-dependent term vanishes at high Reynolds numbers, formula (3.2) also covers *turbulent* flow, where the friction factor is constant over time. Its value will be denoted ζ_{turb}.

As shown in [6], formula (3.1) is not valid for two-phase flow. Instead, it is suggested to use the equation

$$|p_{in}(t) - p_{vap}| \;=\; \frac{1}{2} \cdot \zeta_{2ph} \cdot \rho \cdot u_0(t)^2 \;, \tag{3.3}$$

where p_{vap} is the vapor pressure of the medium and ζ_{2ph} is constant over time.

Following experiences with steady state measurements it is assumed that there is a single transition point where both models (3.1) and (3.3) hold. Consequently, this point is characterized by the value

$$\mathcal{K}_{lim} := \frac{\zeta_{turb}}{\zeta_{2ph}} \,, \tag{3.4}$$

and we expect transition to occur whenever

$$\mathcal{K}_{lim} = \left| \frac{p_{in}(t) - p_{out}(t)}{p_{in}(t) - p_{vap}} \right| . \tag{3.5}$$

As the friction factor $\zeta(t)$ is the quantity to be estimated we have to determine values and confidence intervals of the parameter set

$$\theta := (\zeta_0, \ell, D_0, a, b, c, d, \mathcal{K}_{lim}) \tag{3.6}$$

in the models (3.1) and (3.3). The measured data sets are

$$x_i \;=\; (p_{in}(t), p_{out}(t), A)_i \,,\; 0 \le t \le T_i \,; \quad y_i \;=\; V_i \,; \qquad i = 1, \ldots, n \,,$$

where T_i, A_i, V_i are total cycle duration, smallest orifice cross section area and measured volumes per cycle of dataset i.

So we compute the velocity $u_0(p_{in,i}(t), p_{out,i}(t), \theta, t)$ from (3.1) and (3.3) and then we substitute the model response

$$f(x_i, \theta) := A_i \cdot \int_0^{T_i} u_0(p_{in,i}(t), p_{out,i}(t), \theta, t)\, dt \,, \tag{3.7}$$

into (2.1).

3.2. Measurement error sensitivity. The computation of injected volumes per cycle is very sensitive to the calibration bias. This bias is constant over time and we will denote it α. For time periods Δt where the actual pressure drop $\Delta p = p_{in} - p_{out}$ is relatively small one can estimate the resulting error in the computed volumes per cycle as

$$V(\alpha) = V(0) + \Delta t \cdot \sqrt{\frac{2\,\alpha}{\zeta \cdot \rho}} \tag{3.8}$$

in case of time-invariant friction, e. g. for turbulent flow where friction is independent of the Reynolds number.

From formula (3.8) we expect rather poor signal-to-noise ratios $\Delta p/\alpha$ if Δt is large, which means that our problem may be still ill-posed. At this point, however, we are helped by an advantageous feature of the measured data, which mostly contain the measured data in a small time span Δt.

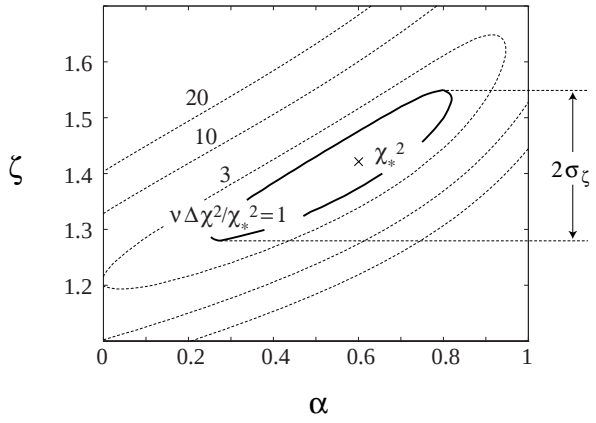

FIG. 3.1. *Expanded confidence regions*

The most simple way of exploiting this, which is sometimes applied in practice, is to introduce a variable lower pressure limit as a decision parameter whether to consider a certain data point or not. We cannot apply this idea here, however, as it introduces a discontinuity. Instead, we smoothly increase ζ for small pressure differences

$$\begin{aligned} \zeta \;&\to\; \zeta + \zeta_{corr} \\ \zeta_{corr} &:= \left(\frac{d}{|p_{in} - p_{out}|} \right)^e , \end{aligned} \tag{3.9}$$

where d is a free parameter and e is a fixed value being determined by the quality of the data.

Formula (3.9) has been designed to maintain an explicit relation for the velocity, which is

$$u_0(p_{in}(t) - p_{out}(t), \alpha, d, e, \zeta_{corr}, t) = \operatorname{sign}(\Delta p(t,\alpha)) \sqrt{\frac{2\,|\Delta p(t,\alpha)|^{e+1}}{\rho\,(A + \zeta_{corr} |\Delta p(t,\alpha)|^e)}} ,$$

with $\Delta p(t,\alpha) = p_{in}(t) - p_{out}(t) + \alpha$.

3.3. Results. In a first series of experiments *orifices with circular cross section* are measured for $n = 26$ different operating points. Their cross section areas A_i range from 0.07 to 0.38 mm^2, and the injected volumes per cycle V_i vary between 20 and 90 mm^2.

It turns out that the most adequate model has a constant friction factor, which reveals that at least a major part of the information is governed by turbulent flow. To identify its value, the correction term (3.9) is needed as otherwise the confidence intervals clearly exceed the physically admissible range. It turns out that $e = 10$ is a good choice and identification yields $d \approx 3$ bar.

Figure 3.1 shows the expanded confidence region (2.3) for $\theta = \zeta$ and $\xi = \alpha$.

Steady-state measurements listed in [5] for about the same range of Reynolds numbers give $\zeta \approx 1.45$. The confidence region in figure 3.1 fits this result very well.

A second measurement series is performed with a *ring shaped orifice* at 20 operating points with different ring width D_0 and length ℓ. We choose this geometry as

it allows very small cross section areas and, consequently, flow at very low Reynolds numbers. Apart from that, only the differences between the lengths ℓ_i of the various operating points are known in advance so that we wish to determine their absolute values.

Step by step expanding and validating the model we see that the full formulation (3.2) is necessary in this case whereas the correction term (3.9) can be omitted.

The Reynolds-dependent term is needed to diminish a trend in the residuals and the geometry factor ℓ/D_0 helps to reduce the variances. The estimated parameters for the Reynolds-dependent term compare to the law of Hagen-Poiseuille for laminar flow. The geometry parameter turns out to be identifiable from the measurements and its value has already been used for the improvement of an RSN-injection nozzle model [13].

The third series gives data of a *nozzle for direct fuel injection*. With these data, the computations using the hydraulic model (3.2) reveal results similar to the first example. In this case, judging from experiences with steady state measurements, cavitation is expected to occur. The expansion of the model by equation (3.3) and introducing $\mathcal{K}_{lim}$ as a free parameter, however, does not lead to a significant improvement of the results [14].

A more detailed description of these results with plots of residuals and confidence regions can be found in [2].

4. Pipe flow.

4.1. Model equations. For the pipe computations we only consider the *averages* of the velocity u, density ρ, pressure p and x-direction shear stress σ over the cross section of the pipe. Further we assume that the temperature is held constant (i. e. there is no energy conservation) and that changes in geodesic height can be neglected. Thus, we arrive at the following differential forms of continuity and momentum conservation laws:

$$\begin{pmatrix} \rho(x,t) \\ \rho(x,t)\,u(x,t) \end{pmatrix}_t + \begin{pmatrix} \rho(x,t)\,u(x,t) \\ \rho(x,t)\,u^2(x,t) + p(x,t) \end{pmatrix}_x = \begin{pmatrix} 0 \\ \sigma(x,t) \end{pmatrix}_x . \tag{4.1}$$

From the second line we subtract u times the first one and then we divide the rest by ρ, which gives

$$\begin{pmatrix} \rho(x,t) \\ u(x,t) \end{pmatrix}_t + \begin{pmatrix} u(x,t) & \rho(x,t) \\ p_x(x,t)/\rho_x(x,t)\rho(x,t) & u(x,t) \end{pmatrix} \cdot \begin{pmatrix} \rho(x,t) \\ u(x,t) \end{pmatrix}_x = \begin{pmatrix} 0 \\ \sigma_x(x,t)/\rho(x,t) \end{pmatrix} ,$$

where we still need to find expressions for the pressure p and the x-direction shear stress σ.

For a pressure relation we need a thermal equation of state. We take the isentropic relation

$$\tilde{\rho}(p(x,t)) \;:=\; \rho(x,t)|_{S=const} . \tag{4.2}$$

For the thermodynamic relation

$$a(\rho(x,t)) \;:=\; \left(\frac{d\tilde{\rho}}{dp}\right)^{-1/2} \tag{4.3}$$

we will use the common notion *isentropic speed of sound*.

For the shear stress we define

$$\frac{\partial \sigma}{\partial x}(x,t) := \rho(x,t) \cdot R(u(x,t),\nu)\,, \tag{4.4}$$

where ν is the kinematic viscosity and $R(u(x,t),\nu)$ is a term developed by Melcher [10] reflecting the dynamic effects of unsteady friction increase:

$$R(u(x,t),\nu) \;=\; \frac{\nu}{A}\int_0^t u_\tau(x,\tau) D(t-\tau)\,d\tau\,. \tag{4.5}$$

Here, A is the pipe cross section area and $D(t)$ is a damping function depending on geometry. For circular cross section we have

$$D(t) = -4\pi \sum_{n=1}^{M} e^{-\omega_n^2 \cdot \nu \cdot t/r^2}\,, \tag{4.6}$$

with r being the pipe radius, ω_n Bessel coefficients and M should be "sufficiently large" (theoretically tending to ∞.)

Consequently, the pipe equations take the form

$$\begin{pmatrix}\rho(x,t)\\ u(x,t)\end{pmatrix}_t + \begin{pmatrix} u(x,t) & \rho(x,t)\\ a^2(\rho(x,t))/\rho(x,t) & u(x,t)\end{pmatrix} \cdot \begin{pmatrix}\rho(x,t)\\ u(x,t)\end{pmatrix}_x \;=\; \begin{pmatrix} 0\\ R(u(x,t),\nu)\end{pmatrix}\,. \tag{4.7}$$

At this point, two simplifying assumptions are made:

1. As the the eigenvalues of the system matrix are $\pm a(\rho(x,t)) + u(x,t)$ while $|u(x,t)| \ll |a(\rho(x,t))|$ the diagonal entries $u(x,t)$ are supposed not to influence the system's behavior significantly and are thus neglected. This assumption seems to be feasible due to our experiences [2].

2. According to acoustic theory the left-hand side of the system is linearized about some state ρ. Later on we will point out some limitations of this assumption, but meanwhile we remain faithful to it.

Using these assumptions to first linearize the system and then to rewrite it in terms of p we derive the linear "equations of ALLIEVI", which are commonly used in hydraulic simulation:

$$\begin{pmatrix}p(x,t)\\ u(x,t)\end{pmatrix}_t + \begin{pmatrix} 0 & a^2\rho\\ 1/\rho & 0\end{pmatrix} \cdot \begin{pmatrix}p(x,t)\\ u(x,t)\end{pmatrix}_x \;=\; \begin{pmatrix} 0\\ R(u(x,t),\nu)\end{pmatrix}\,. \tag{4.8}$$

Together with initial conditions

$$p(x,0) = p_0(x) \tag{4.9}$$
$$u(x,0) = u_0(x) \tag{4.10}$$

and two of the boundary conditions

$$p(0,t) = p_A(t) \tag{4.11}$$
$$p(x_L,t) = p_E(t) \tag{4.12}$$
$$u(0,t) = q_A(t)/A \tag{4.13}$$
$$u(x_L,t) = q_E(t)/A \tag{4.14}$$

the equations (4.8) with the friction model (4.5) give an integro differential initial boundary value problem of the Volterra type, where a and ν are the parameters to be estimated.

4.2. Solution of the pipe equations. In engineering praxis, a common attempt to solve the equation (4.8) is to set $R(u(x,t),\nu) \equiv 0$, which makes it easy to decouple the system and solve it ("D'Alembert's solution"). The resulting pressure signals are then multiplied by an exponential damping term (e. g. *see* [1]). This strategy, however, leads to results that substantially violate mass conservation as shown in [15]. Moreover, the damping parameter has no physical interpretation, which makes it hard to verify its estimate.

Fortunately, a very efficient algorithm has been developed by Michael Kroller [7]. It takes advantage of the analytical solution of the initial boundary value problem (derived by Laplacian transformation):

$$\begin{aligned} q_A(t) \;=\; & \frac{A}{a\cdot\rho}\,p_A(t) \;-\; \frac{A\cdot\widehat{a_o}}{a\cdot\rho}\,p_E(t-x_L/a)h(t-x_L/a) \;+ \\ & +\; \widehat{a_o}\cdot q_E(t-x_L/a)h(t-x_L/a) \;-\; A\cdot\mathcal{I}_1(t) \;- \\ & -\; \frac{A\cdot\widehat{a_o}}{a\cdot\rho}\cdot\mathcal{I}_2(t-x_L/a)h(t-x_L/a) \;+\; A\cdot\widehat{a_o}\cdot\mathcal{I}_3(t-x_L/a)h(t-x_L/a) \end{aligned} \tag{4.15}$$

$$\begin{aligned} q_E(t) \;=\; & \frac{A}{a\cdot\rho}\,p_E(t) \;+\; \frac{A\cdot\widehat{a_o}}{a\cdot\rho}\,p_A(t-x_L/a)h(t-x_L/a) \;+ \\ & +\; \widehat{a_o}\cdot q_A(t-x_L/a)h(t-x_L/a) \;-\; A\cdot\mathcal{J}_1(t) \;+ \\ & +\; \frac{A\cdot\widehat{a_o}}{a\cdot\rho}\cdot\mathcal{J}_2(t-x_L/a)h(t-x_L/a) \;+\; A\cdot\widehat{a_o}\cdot\mathcal{J}_3(t-x_L/a)h(t-x_L/a)\;, \end{aligned} \tag{4.16}$$

where

$$\begin{aligned} \widehat{a_o} \;&=\; e^{\,x_L\cdot\nu/(2a\cdot A)}D(0) & h(t) \;&=\; \begin{cases} 1 & t\geq 0 \\ 0 & t<0 \end{cases} \\ \mathcal{I}_1(t) \;&=\; \frac{1}{A}\int_0^t c_1(t-s)q_A(s)\,ds & \mathcal{J}_1(t) \;&=\; \frac{1}{A}\int_0^t c_1(t-s)q_E(s)\,ds \\ \mathcal{I}_2(t) \;&=\; \int_0^t c_2(t-s)p_E(s)\,ds & \mathcal{J}_2(t) \;&=\; \int_0^t c_2(t-s)p_A(s)\,ds \\ \mathcal{I}_3(t) \;&=\; \frac{1}{A}\int_0^t c_3(t-s)q_E(s)\,ds & \mathcal{J}_3(t) \;&=\; \frac{1}{A}\int_0^t c_3(t-s)q_A(s)\,ds\;. \end{aligned}$$

The functions $c_1(t)$, $c_2(t)$ and $c_3(t)$ are defined by their Laplace transforms

$$\tilde{c_1}(s) \;=\; \sqrt{1-\frac{\nu}{A}\tilde{D}(s)} \;-\; 1 \tag{4.17}$$

$$\tilde{c_2}(s) \;=\; -1 \;+\; e^{\,-x_L\cdot s\cdot\tilde{c_1}(s)/a}/\widehat{a_o} \tag{4.18}$$

$$\tilde{c_3}(s) \;=\; \tilde{c_1}(s)\cdot\tilde{c_2}(s) \;+\; \tilde{c_1}(s) \;+\; \tilde{c_2}(s) \tag{4.19}$$

where

$$\tilde{D}(s) \;=\; -4\pi\sum_{n=1}^{M}\frac{1}{s+\omega_n^2\cdot\nu/r^2}\,. \tag{4.20}$$

For $c_1(t)$, $c_2(t)$ and $c_3(t)$ the approximations

$$c_1^*(t) \;=\; -\,\frac{\nu}{2A}D(t) \;-\; \frac{\nu^2}{8A^2}(D*D)(t) \tag{4.21}$$

$$c_2^*(t) \;=\; \frac{x_L}{a}\,[\,\frac{\nu}{2A}D'(t) \;+\; \frac{\nu^2}{8A^2}\,((D'*D)(t)+D(0)D(t))\,] \tag{4.22}$$

$$c_3^*(t) \;=\; c_2^*(t) \;-\; \frac{\nu}{2A}D(t) \tag{4.23}$$

are implemented by efficient recursion formulae as shown in [7].

After some tedious rearranging of terms we arrive at a formula that allows the computation of pressure and velocity at a third position x_M (*see* also [2]):

$$\begin{aligned} p_M(t) \;=\; \frac{1}{2}\,(\,\mathcal{K} - \frac{a\cdot\rho}{A\cdot\widehat{a_o}}\,q_A(t+x_M/a) \;+\; \frac{1}{\widehat{a_o}}\,p_A(t+x_M/a) \;-\\ -\;\frac{a\cdot\rho}{\widehat{a_o}}\,\mathcal{I}_1 \;-\; \mathcal{I}_2 \;+\; \frac{a\cdot\rho}{A}\,\mathcal{I}_3\,) \end{aligned} \tag{4.24}$$

$$q_M(t) \;=\; \frac{A}{a\cdot\rho}\;(\mathcal{K} \;-\; p_M(t)) \tag{4.25}$$

where

$$\begin{aligned} \mathcal{K} \;=\; \widehat{a_o}\cdot p_A(t-x_M/a)h(t-x_M/a) \;+\; \frac{a\cdot\rho\cdot\widehat{a_o}}{A}\,q_A(t-x_M/a)h(t-x_M/a) \;-\\ -\;a\cdot\rho\cdot\mathcal{J}_1(t) \;+\; \widehat{a_o}\cdot\mathcal{J}_2(t-x_M/a)h(t-x_M/a) \;+\\ +\;a\cdot\rho\cdot\widehat{a_o}\cdot\mathcal{J}_3(t-x_M/a)h(t-x_M/a)\;. \end{aligned}$$

In order to validate the results, a considerable sample of test was also computed with general purpose time-marching schemes of first order (like the method of characteristics). In most cases, the approximations (4.21, 4.22, 4.23) proofed to be sufficiently accurate. Theoretical error estimates are given in [7] and numerical results are shown in [2]. Significant inaccuracies only occur at extremely long pipes (we sometimes use such pipes in order to get more accurate parameter estimates.) In these cases, it suffices to add higher order terms to the approximations (4.21) through (4.23).

4.3. Estimation procedure and results. Measurements are taken for the boundary conditions (4.11) and (4.12) and the interior pressure signal p_{mea}, the latter being the observation to be compared with the computed signal p_M from (4.24).

From the equations (4.15, 4.16, 4.24 and 4.25) we observe that the significant parameters to be identified are $\tau := x_L/a$ and ν. The density parameter ρ is just a scaling factor of the velocities. Consequently, it cannot be identified from the pressure measurements. Of course, one has to keep that in mind when interpreting the computed velocity information.

The parameters are estimated by the minimization

$$\min_{\tau,\nu}\;\int_0^T\;\left(p_M(t,\tau,\nu)-p_{mea}(t)\right)^2\;dt\;. \tag{4.26}$$

Measurements have been taken at a wide range of operating points (load and speed) of the injection pump. In contrast to the investigation of the orifice, however, the pipe parameters can be identified based on the measurements of a single operating point.

At the end of the pipe there is either

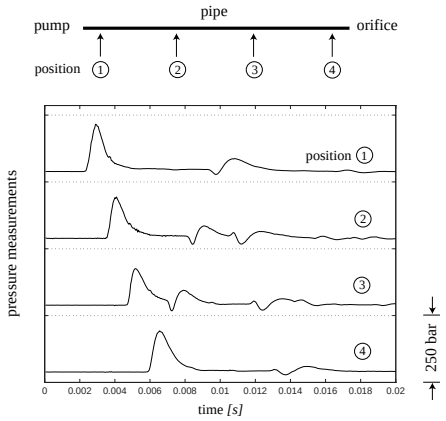

FIG. 4.1. *Measurement example (diesel)*

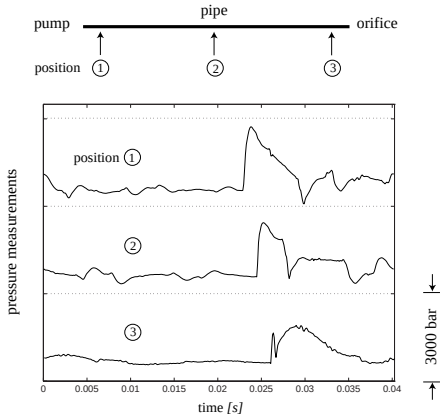

FIG. 4.2. *Measurement example (dimethyl ether)*

- a nozzle with five sprayholes,
- an orifice with circular cross-section or
- a ring-shaped orifice.

Most of the measurements have been performed with diesel and some with dimethyl ether. They have been taken at four positions along the injection line. Consequently, there are several combinations of p_A, p_{mea} and p_E, which yields an additional possibility to check the results. Measurement examples are given in figures 4.1 and 4.2.

From the results we have observed the following:

1. Some of the measurements are biased by cavitation phenomena, which is not adequately represented in the model. These data sets, however, are easily recognized by their significantly different parameter estimates. We tried to catch these phenomena by means of cavities of varying size at fixed positions in the flow, but this did not lead to any meaningful result. More sophisticated models will have to be developed for that purpose.

2. In the purely hydraulic case it turned out that the estimates for τ significantly depend on the pressure average of the measured data. Consequently, we feel that the *pointwise* dependence $a(p)$ should be considered in a future pipe model.

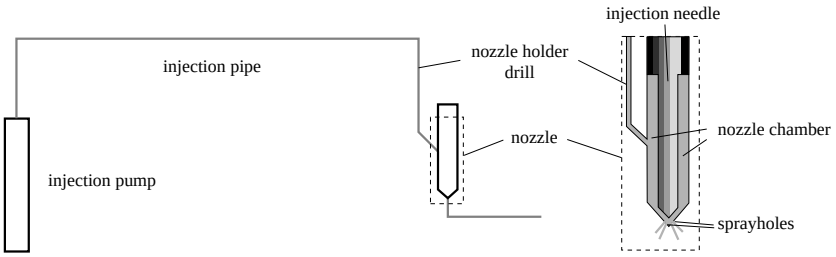

FIG. 5.1. *Line-nozzle system*

3. Slightly distorted values of τ tend to cause oscillations in the computed pressure signals. Thus there is a strong covariance between τ and ν as the latter may damp these oscillations.

4. Near the pump lower values of ν are identified. This may be due to the temperature drop along the line. Maybe this means that one should assign greater values for the nozzle holder flow viscosity (*see* also next section).

5. Influence of numerical diffusion seems to be significant in some cases where identified kinetic viscosity of the diverse numerical algorithms varies significantly. Therefore, it should be worthwhile to recompute everything with a scheme of order greater than one. As spurious oscillations of higher order schemes may also lead to significantly biased estimates for kinetic viscosity, it will be important to choose this scheme carefully.

6. In general, the estimates for diesel fuel seem to be much more reliable than those for dimethyl ether. This is not surprising in view of the quality of measured signals (*see* the figures 4.1 and 4.2.)

Tables of identified parameters are given in [2].

5. Line-nozzle system. We want to conclude the paper with a few ideas for the analysis of a full line-nozzle system based on the methods described above. A schematic illustration of this system is given in figure 5.1.

To maintain simplicity, we assume that the injection needle is in a fixed position (a dynamic mass-and-spring model extending this setup with a moving needle can be found in [2].) The injection pipe, the nozzle holder drill and the nozzle chamber are described by means of the pipe model. The energy losses at needle seat and sprayholes follow the ring-shaped orifice and the nozzle models.

In a standard setup, dynamic pressure measurements can be placed along the injection pipe and at the nozzle outlet. In addition, we have measurements of total fuel volume per injection cycle. We know the length of the injection pipe and the size of nozzle chamber, needle seat (maybe determined by the parameter estimation approach presented in §2 and [13]) and sprayholes. The exact length of the nozzle holder drill, however, is usually not given.

Our proposed strategy is now divided in two steps:

1. We identify viscosity and sonic speed from at least three pressure measurements along the injection pipe and compute the corresponding flow velocities applying the methods of §4.

2. We use the line model and the identified parameters to compute the flow through nozzle holder drill and nozzle chamber (the latter could also be computed rather accurately via the integrated continuity equations, but we find that this procedure is not numerically stable, *see* [2]), which yields sprayhole inlet pressure and

flow velocity.

The feasibility of the first step depends on the model (*see* the discussion in the previous chapter) and the sharpness of the estimates. If the confidence regions are too large, we will have to admit that the information we can get about the full system is rather limited.

We now draw our attention to the second step, where the unknown length of the nozzle holder drill is the major problem. Let us first collect some observations we made about our computations.

The first observation is that the *time-integrated* computed velocity signal (i. e. the computed volume per cycle) is not sensitive to the assumed length of the nozzle holder drill. It is, however, very sensitive to the nozzle holder flow viscosity, which therefore can be identified very sharply.

The second observation is that the *shape* of the computed velocity signal heavily depends on the length of the nozzle holder drill and, correspondingly, on the sonic speed a identified by means of the methods of §4. Here, again, our doubts about the constant speed of sound assumptions come into play. If there is any significant dependency $a(p)$ along the pipe and the nozzle holder drill model improvement will be indispensibel for accurate computation of the velocity signal with the currently used models.

The latter observation and the fact that one cannot just naïvely assign the inlet velocity to the sprayhole velocity u_0 via the diameter ratio directly lead to similar conclusions about the determination of the orifice's $\zeta(t)$ by means of the simplified equations (3.1) and (3.3).

The third observation is that the computed nozzle inlet *pressure* signals are far less sensitive to sonic speed and nozzle holder drill length than the velocity signals are.

Therefore, we suggest the following procedure to identify $\zeta(t)$:

1. Given at least three pressure measurements identify flow viscosity and sonic speed along the pipe by means of the methods described in §4.
2. Identify the flow viscosity along the nozzle holder using the measured volumes per cycle.
3. Use the identified quantities and a rough estimate of the nozzle holder drill length to compute the pressure at the sprayhole inlet.
4. Perform steps 1–3 for a sufficient amount of operating points. Given the measured volumes per cycle and outlet pressure signals one can now identify $\zeta(t)$ by means of the methods of §3.

REFERENCES

[1] W. Bosch, *Untersuchungen zur instationären reibenden Strömung in Druckleitungen von Einspritzsystemen*, tech. rep., Ber. Nordrhein-Westf., Nr. 987, 1961.

[2] W. Egartner, *Parameterschätzung in eindimensionalen Modellen für instationäre Strömung in Dieseleinspritzsystemen*, PhD thesis, Graz University of Technology (Erzherzog-Johann-Universität Graz), 1996.

[3] T. Gruber, *Bestimmung der Widerstandscharakteristik am Nadelsitz einer Einspritzdüse*, Master's thesis, Fachbereich Physikalische Ingenieurwiss., TU Berlin, Oct. 1993.

[4] H. Hiroyuki, *Diesel engine combustion and its modelling; diagnostics and modelling of combustion in reciprocating engines*, COMODIA, (1985).

[5] I. E. Idelchik, *Handbook of Hydraulic Resistance*, Springer Verlag, 2 ed., 1986.

[6] P. Kapus and H. Ofner, *Developement of fuel injection equipment and combustion system for DI diesels operated on dimethyl ether*, in SAE 950062, 1995.

[7] M. Kroller, *Efficient computation of a mathematical model for the damping of pressure waves in tubes of circular form*, Numerical Methods for Partial Differential Equations, 11 (1995), pp. 41–60. John Wiley & Sons.

[8] M. Marcic, *Calculation of the diesel fuel injection parameters*, in SAE 952071, Detroit, 1995.

[9] D. W. Marquardt, *An algorithm for least-squares estimation of nonlinear parameters*, J. Soc. Indust. Appl. Math., 11 (1963), pp. 431–441.

[10] K. Melcher, *Ein Reibungsmodell zur Berechnung von instationären Strömungen in Rohrleitungen an Brennkraftmaschinen*, Bosch Techn. Berichte, 4 (1974), pp. 273–290.

[11] J. J. Moré, *The Levenberg-Marquardt algorithm: implementation and theory.*, in Numer. Anal., Proc. bienn. Conf., Dundee, 1977.

[12] J. J. Moré, B. S. Garbow, and K. E. Hillstrom, *User guide for MINPACK-1*, tech. rep., Argonne National Laboratory Report ANL-80-74, 1980.

[13] *Neue Dieseleinspritzdüse für optimalen Einspritzverlauf*, MTZ, (1995).

[14] H. Ofner and W. Egartner, *Identification of flow phenomena in fuel injection systems for diesel engines from dynamic measurements*, in IMechE Computers in Engine Technology C499/053, London, 1996.

[15] H. Ofner and D. W. Gill, *A general purpose simulation model for high pressure fuel injection and other mechanical-hydraulic systems*, in IMechE Computers in Engine Technology C430/009, London, 1991.

[16] W. H. Press, S. A. Teukolsky, W. T. Vetterling, and B. P. Flannery, *Numerical Recipes in C, The Art of Scientific Computing*, Cambridge Univ. Press, 2 ed., 1992, ch. 15.6, pp. 693+.